

LIQUID CRYSTAL ELASTOMERS AND PHASE TRANSITIONS IN ACTIN ROD NETWORKS*

M. CARME CALDERER[†], CARLOS A. GARAVITO GARZÓN[†], AND CHONG LUO[†]

Abstract. In this article, we construct and analyze models of anisotropic crosslinked polymers employing tools from the theories of nematic liquid crystals and liquid crystal elastomers. The anisotropy of these systems stems from the presence of rigid rod molecular units in the network. We construct energy functionals for compressible and incompressible elastomers as well as for rod-fluid networks. The theorems on the minimization of these energies combines methods of isotropic nonlinear elasticity with the theory of lyotropic liquid crystals. Two of the theorems refer to incompressible elastomers, in the cases that the bulk liquid crystal energy is given by the well-known polynomial form of the Landau–de Gennes theory and also in the case of a singular potential. Another theorem refers to compressible elastomers, and in the last row, the rod density is taken as a main field of the model. We apply our results to the study of phase transitions in networks of rigid rods, in order to model the behavior of actin filament systems found in the cytoskeleton. Our results show a good agreement with the molecular dynamics experiments reported in the literature as well as with some laboratory experiments. The model does not include polydispersity effects due to variable rod shape and size, and it does not account either for phase transitions to lamellar phases.

Key words. variational methods, energy minimization, liquid crystals, nonlinear elasticity, anisotropy, phase change, networks, actin

AMS subject classifications. 70G75, 74G65, 76A15, 74B20, 74E10, 80A22

DOI. 10.1137/130914309

1. Introduction. Cytoskeletal networks consist of rigid, rodlike actin protein units jointed by flexible crosslinks, presenting coupled orientation and deformation effects analogous to liquid crystal elastomers. The alignment properties of the rigid rods influence the mechanical response of the network to applied stress and deformation, affecting functionality of the systems [40], [24]. Parameters that characterize these networks include the aspect ratio of the rods and the average length of the crosslinks, with a large span of parameter values found across in vivo networks. For instance, cytoskeletal networks of red blood cells have very large linkers and small rod aspect ratio [39], [23], whereas those of cells found in the outer hair of the ear have a very large aspect ratio and short linkers favoring a well-aligned nematic, in order to achieve an efficient sound propagation [29]. This article is motivated by the works on Monte Carlo simulations of phase transitions in rigid rod fluids by Bates and Frenkel [6] and the later application to actin networks by Dalhaimer, Discher, and Lubensky [14]. In these articles, the authors discuss experimentally observed alignment states and their phase transitions as well as predictions from numerical experiments. They report on a wide range of anisotropic regimes, including the uncrosslinked fluid network, in the nematic as well as the isotropic state, and the crystal-glass states involving elastomer microstructure. A goal of our work is to obtain a continuum model matching predictions of the molecular simulations and available experiments.

A nematic fluid consists of interacting rodlike molecules that have the tendency to align along preferred directions and the ability to flow under applied forces. Liq-

*Received by the editors March 25, 2013; accepted for publication (in revised form) February 25, 2014; published electronically May 15, 2014. This research was partially supported by a grant from the National Science Foundation, NSF-DMS 0909165.

<http://www.siam.org/journals/siap/74-3/91430.html>

[†]School of Mathematics, University of Minnesota, Minneapolis, MN 55455 (calde14@umn.edu, garav007@umn.edu, luochong@gmail.com).

liquid crystal elastomers are anisotropic nonlinear elastic materials, with the source of anisotropy stemming from elongated, rigid monomer side groups, or from main chain rodlike elements. They are elastic solids that may also present fluid regimes of [13] (see [15], [16], [21], [41]). The interaction between the rod units and the network is at the core of liquid crystal elastomer behavior. In *main chain* elastomers, the connected rigid units are part of the backbone chains of the system and in *side chain* elastomers, the rod units are attached to the polymer backbone. In both cases, the backbone chains are crosslinked into a network. Models of anisotropic polymer melts and their non-Newtonian behavior have received significant attention [19], [38], [42].

Ordering in nematic fluids is affected by temperature in thermotropic liquid crystals and by rod concentration in lyotropic ones. At high temperature or low concentration, respectively, nematic fluids are found in the isotropic state, experiencing a transition to the nematic upon cooling the thermotropic liquid or increasing the rod concentration of the lyotropic [25]. In rodlike systems, such as actin fiber networks, the phase transition behavior is affected by the density of rods.

We consider anisotropic systems such that the total energy is the sum of the Landau–de Gennes liquid crystal energy of the nematic and an anisotropic elastic stored energy function. This energy involves two sources of anisotropy expressed by symmetric second order tensors, that associated with the rigid units, represented by the nematic order tensor Q , and that of the network described by the positive definite, step-length tensor L , which encodes the shape of the network: it is spherical for isotropic polymers and spheroidal for uniaxial nematic elastomers, and has eigenvalues l_{\parallel} and l_{\perp} (double). The quantity $r := \frac{l_{\parallel}}{l_{\perp}} - 1$ measures the degree of anisotropy of the network, with positive values corresponding to prolate systems and negative ones to the oblate shapes. In the prolate geometry, the eigenvector \mathbf{n} associated with l_{\parallel} is the director of the theory, giving the average direction of alignment of the rods and also the direction of shape elongation of the network. It is natural to assume that L and Q share eigenvectors. In particular we assume that they are linearly related, so that for L prescribed, we take Q as its traceless version, that is $Q = L - \frac{1}{3}\text{tr}LI$ [41, p. 49]. The free energy may also carry information on the anisotropy L_0 imprinted in the network at crosslinking the original polymer melt. In this work, we assume that L and Q are defined on the reference configuration Ω of the elastomer.

The Landau–de Gennes free energy density is the sum of scalar quadratic terms of ∇Q and the bulk scalar function $f(Q)$. In the de Gennes–Landau theory, f is a polynomial function of the trace of powers of Q and describes the phase transition between the isotropic and the nematic phases [25]. However, the polynomial growth is not physically realistic since it is expected that an infinite energy should be required to reach limiting alignment configurations [8], [18]. This turns out to be, as well, an essential element of our analysis that we formulate as the blow-up of f as the minimum eigenvalue, $\lambda_{\min}(Q)$, approaches $-\frac{1}{3}$ [33], [5]. In the latter article, the authors show that, in the case of thermotropic liquid crystals, the asymptotic behavior of f is required to guarantee the compatibility of the Maier–Saupe energy and the continuum theory. A cautionary note about notation: we will employ the common symbol f to denote the bulk nematic energy density in the different cases that we address.

Denoting F the deformation gradient, the elastic energy density proposed by Bladon, Terentjev, and Warner is $|L^{-\frac{1}{2}}FL_0^{\frac{1}{2}}|^2$. It is the analog of the neo-Hookean energy of isotropic elasticity, and also derived from Gaussian statistical mechanics. Taking into account the relevant role played by the tensor $G := (L^{-1}FF^TL_0)^{\frac{1}{2}}$ in the trace form of the energy, and motivated by the theory of existence of minimizers

of isotropic nonlinear elasticity [4], we consider polyconvex stored energy density functions $W(\mathbf{X}) = \hat{W}(G(\mathbf{X}))$, $\mathbf{X} \in \Omega$. However, since G is not a gradient, we must be able to recover the limiting deformation gradient F^* from the minimizing sequences $\{G_k\}_{k \geq 1}$. For this, it is necessary that the minimizing sequences $\{L_k\}$ yield a nonsingular limit. This is achieved, by either restricting the range of the eigenvalues of Q in the admissible set so that $\lambda_{\min}(Q)$ is strictly greater than $-\frac{1}{3}$, or by requiring the blow up of $f(Q)$ at the lower eigenvalue limit. The former enters in the first theorem on existence of a minimizer of the incompressible elastomer (Theorem 3.4), in the case of polynomial bulk energy $f(Q)$. We believe that this case merits special treatment, since the polynomial form of $f(Q)$ is used in the vast majority of the research carried out in the scientific community involving the Landau–de Gennes energy. The assumption of f being a singular potential is made in our second theorem on existence of a minimizer of the incompressible elastomer energy (Theorem 3.5) as well as in the compressible (Theorem 3.6) and rod-network cases (Theorem 3.7) and (Theorem 3.8). The simulations presented in section 4 are also based on the singular potential that we construct.

In the case of compressible networks, we further assume that mechanical expansion and compression are coupled with liquid crystal order, so that the bulk free energy is now $f(Q, \det F)$. Following the analogous assumptions of isotropic elasticity, we require that, for each symmetric traceless tensor Q , f becomes unbounded as $\det F \rightarrow \{0, \infty\}$. We argue that the coupling between expansion and compression with nematic order is qualitatively analogous to that of lyotropic uniaxial nematic liquid crystals, as proposed by Kuzuu and Doi [31]. In this case, the bulk energy $f(s)$ is parametrized by the rod concentration of the nematic fluid. At low concentration, the isotropic minimum dominates, with nematic becoming the preferred phase as the concentration increases. In the application to rigid rod networks of section 4, two parameter rates emerge as very relevant: $\chi = \frac{L_a}{L_x}$, where L_a denotes the typical length of a cylindrical rod, and L_x that of a crosslinker filament, and the aspect ratio $A_a = \frac{L_a}{D_a}$ of the rod, where D_a denotes a typical diameter. We assume that f depends on s and the rigid rod density ρ , and it is also parametrized by the ratio χ . Specifically, following the denominations of *loose*, *semiloose*, and *tight* for networks with small through large values of χ , we assume that f evolves from a function with a single isotropic well for χ small (large linkers), to having a single nematic well for large χ (short linkers), presenting an intermediate double-well region. We also assume that the liquid energy scales according to the aspect ratio of the rods, resulting in larger nematic contribution with increasing aspect ratio. Proposition 4.1 summarizes the results on phase transitions under three-dimensional expansion. In subsection 4.2.1, we construct a bulk free energy density with the previously described properties and present results on numerical simulations of the phase transition behavior under plane extensions, plots of phase diagrams in the density-aspect ratio plane, and the graphs of the equilibrium order parameter s with respect to the rod density. In particular, we find oblate equilibrium states for small values of the aspect ratio, corresponding to disklike molecules.

We point out that in the theorems of section 3, we assume the deformation map $\varphi \in W^{1,p}(\Omega, \mathbb{R}^n)$, with $p \geq 2$. This assumption helps in simplifying the proofs. However, in the case of three space dimensions, it is well known that $2 \leq p \leq 3$ does not guarantee injectivity of the minimizer map φ^* . Consequently, in the points of the domain where injectivity fails (perhaps due to formation of cavities in the material or boundary self-contact), it is not possible to define the Eulerian *pull-forward* tensor maps $Q(\mathbf{x}) = Q(\mathbf{X}^{-1}(\mathbf{x}))$, $L(\mathbf{x})$, as well as $\rho(\mathbf{x})$. In particular, the latter is needed

to interpret (3.34) as the equation of balance of the mass of rods. Likewise, this also prevents us from interpreting the Landau–de Gennes contribution terms in the energy functionals (2.6), (2.7), and (2.8) in the Eulerian frame, as it might be suggested by the *liquidlike* character of the Landau–de Gennes energy. This is due to the fact that the change of volume formula does not hold in the absence of injectivity of the deformation map. From a related point of view, we justify the Lagrangian expression $|\nabla Q|^2$ in the energy as a result of the scaling properties of the energy as stated in Remark 4. Moreover, our proposed form is exact for small strain deformations (with large rotations allowed).

In addition to the trace models of liquid crystal elastomer energy studied by Warner and Terentjev ([41] and references therein), generalizations of these earlier forms have been proposed and studied by several authors ([2] and [20]; [1], [10], [11], and [17]). In the first two references, the authors propose energies based on powers of the earlier trace form, including Ogden-type energies, and study their extensions to account for semisoft elasticity. Articles by de Simone et al. also propose and study Ogden-type energies. Furthermore, the analysis of equilibrium states presented in [1] applies to elastomer energy density functions that are not quasi-convex. (For instance, these are appropriate to model crystallike phase transitions.) Their methods of proof combine the construction of lower quasi-convex envelopes, the rigidity theorem [22], and tools from the theory of Γ -convergence. Our results apply to a more restrictive class of energy density functions, that is, polyconvex functions with respect to the anisotropic deformation tensor G . Our methods of proof use tools of isotropic nonlinear elasticity, and as such, are directly tailored to treating polyconvexity. Moreover, this approach readily applies to modeling the nonconvexity associated with nematic liquid order in networks and the corresponding phase transitions, although it does not cover the more general type of transitions linked to quasi-convexity. The article [35] presents a finite element analysis of the trace model, including simulations of domain formation under extension and stress-strain graphs that characterize the semisoft elastic response.

This article is organized as follows. Section 2 starts with the formulation of the energy functionals to be analyzed, which include the incompressible and compressible liquid crystal elastomers as well as a rod–fluid network model. The anisotropy sources of the systems are discussed and rigorously formulated. The main issues addressed include the constitutive equations, linking the polymer anisotropy represented by the tensor L and the liquid crystal order measured by Q , the coupling of volume change and order encoded in the bulk liquid crystal energy f , the polynomial dependence of f on Q versus the singular potential assumption, the scaling property of the term $|\nabla Q|^2$ and its mathematical justification, and the choice of the Lagrangian frame, the related regularity requirements on the admissible sets, and the issue of injectivity of the deformation map. Section 3 is devoted to the statement and proof of 5 theorems on the minimization of the energy functionals. The first two theorems refer to incompressible elastomers in the cases that $f(Q)$ is a polynomial and a singular potential, respectively. Another of the theorems applies to a compressible elastomer, whereas the last two explicitly consider the source of compressibility as a result of changes of density of the rigid rods. Section 4 presents a study of density dependent liquid crystal phase transitions, with figures corresponding to the phase transition diagram and the order properties with respect to mechanical extension of the system. The conclusions are described in section 5. Auxiliary results employed in the proofs of existence of a minimizer have been included in the appendix. Some of the results of section 3 find their motivation in the Ph.D. thesis dissertation by Luo [33].

Finally, we introduce some notation and basic definitions used in the paper. We let the open and bounded domain $\Omega \subset \mathbf{R}^n$, $n = 2, 3$, with sufficiently smooth boundary, denote the reference configuration of the elastomer. Let \mathbb{M}^3 denote the space of second order tensors and

$$\begin{aligned}
 (1.1) \quad & \mathbb{M}_+^3 = \{M \in \mathbb{M}^3 : \det M > 0\}, \quad \mathbb{M}_{+1}^3 = \{M \in \mathbb{M}^3 : \det M = 1\}, \\
 & \mathbb{S}^3 = \{M \in \mathbb{M}^3 : M = M^T\}, \\
 (1.2) \quad & \mathbb{S}_+^3 = \{M \in \mathbb{S}^3 : \det M > 0\}, \quad \mathbb{S}_0^3 = \{Q \in \mathbb{S}^3 : \text{tr } Q = 0\}, \\
 & \mathcal{Q}_0^+ = \left\{ Q \in \mathbb{S}_0^3 : \lambda_{\min}(Q) > -\frac{1}{3} \right\}.
 \end{aligned}$$

2. The Landau–de Gennes liquid crystal elastomer. In order to state the energy functionals to be analyzed, we first present the dependent fields of the problem. The *deformation map* of the polymer and its gradient, respectively, are given by

$$\begin{aligned}
 (2.1) \quad & \varphi : \Omega \longrightarrow \bar{\Omega}, \quad \mathbf{x} = \varphi(\mathbf{X}), \\
 & F = \nabla \varphi, \quad \det F > 0,
 \end{aligned}$$

$\bar{\Omega} = \varphi(\Omega)$. Equilibrium states of nematic liquid crystal elastomers are characterized by the deformation map φ , the *step tensor* and the *order tensor* fields, $L : \Omega \longrightarrow \mathbb{S}_+^3$ and $Q : \Omega \longrightarrow \mathbb{S}_0^3$ describing the shape of the network and the nematic order of the rigid units, respectively. The reference configuration is characterized by the fields L_0 and $Q_0 \in \mathbb{S}_0^3$, and, in some cases, by the density $\rho_0 = \rho_0(\mathbf{X})$ of rigid rods.

A relevant quantity of the theory is the *effective deformation tensor*

$$(2.2) \quad G = L^{-\frac{1}{2}} F L_0^{\frac{1}{2}}.$$

Associated with the postulated material fields L and Q , we consider their Eulerian counterparts $\bar{L}(\mathbf{x}) = L(\varphi^{-1}(\mathbf{x}))$ and $\bar{Q}(\mathbf{x}) = Q(\varphi^{-1}(\mathbf{x}))$, respectively. These are well defined provided φ is injective, as discussed in Remark 6. The interpretation of relation (2.2), based on ideas of plasticity and justified by the statistical theory of polymers, is illustrated in Figure 1. Given functions

$$(2.3) \quad \hat{W} : \mathbb{M}_+^3 \longrightarrow \mathbb{R},$$

$$(2.4) \quad f, \hat{f} : \mathbb{M}_+^3 \times \mathbb{R}^+ \longrightarrow \mathbb{R},$$

$$(2.5) \quad g : \mathbb{R}^+ \longrightarrow \mathbb{R},$$

we let $W(\mathbf{X}) = \hat{W}(G(\mathbf{X}))$ represent the elastic free energy density, and $f(\mathbf{X}) = f(Q(\mathbf{X}), \det F(\mathbf{X}))$ and $\hat{f}(\mathbf{X}) = \hat{f}(Q(\mathbf{X}), \rho(\varphi(\mathbf{X})))$ denote bulk liquid crystal energy densities of the material, the latter in terms of the rod density. In the case that the material is incompressible, we use the notational convention $f(Q)$ to denote the restriction $f(Q, 1)$. Also, for the sake of simplicity, we treat the material as homogeneous, with the extension to the inhomogeneous case being routine.

For given material parameters $\mu \geq 0, \nu \geq 0$, and $k \geq 0$, the main types of energy functionals treated in this work are the following.

1. Compressible liquid crystal elastomer:

$$(2.6) \quad \mathcal{E} = \int_{\Omega} \left[\frac{\mu}{2} (\hat{W}(G) + g(\det F)) + \nu f(Q, \det F) + k |\nabla Q|^2 \right] d\mathbf{X}.$$

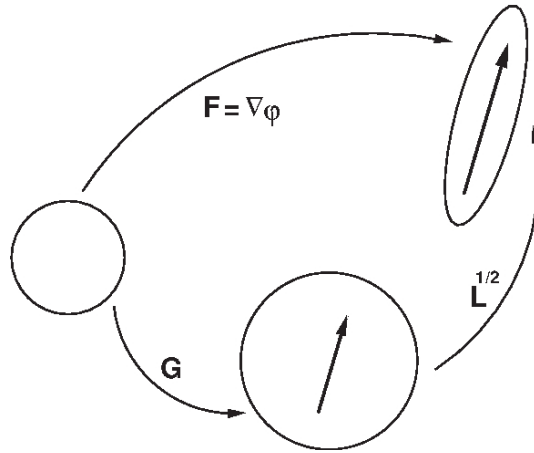


FIG. 1. Decomposition $F = L^{\frac{1}{2}}G$, G representing an effective deformation tensor, that is, the deformation experienced by an isotropic material. The superposed soft mode deformation $L^{\frac{1}{2}}$ indicates the bias along the preferred direction, represented by the arrow. The special case of an isotropic reference configuration (blank circle) $L_0 = I$ is shown.

2. Incompressible liquid crystal elastomer:

$$(2.7) \quad \mathcal{E} = \int_{\Omega} \left(\frac{\mu}{2} \hat{W}(G) + \nu f(Q) + k |\nabla Q|^2 \right) d\mathbf{X}.$$

3. Network of rigid rods:

$$(2.8) \quad \mathcal{E} = \int_{\Omega} \left[\frac{\mu}{2} (\hat{W}(G) + g(\det F)) + \nu \hat{f}(Q, \rho) + \varepsilon |\nabla \rho|^2 + k |\nabla Q|^2 \right] d\mathbf{X}.$$

Remark 1. Here, we take a simplified form of the energy expression involving ∇Q and $\nabla \rho$. In the article [26], the authors give a full derivation of the energy, according to the Onsager model for sphero-cylinder particles, listing all the terms that couple the rod density with Q .

Next, we discuss the mechanical and liquid crystal coupling terms in the energy, the classical ones as well as those that are original to this work, and establish their mathematical properties.

2.1. Statistical mechanics of anisotropic polymers. We now focus on the statistical treatment of single ideal chains, following the development in [41]. Let us consider a freely jointed chain composed of N segments of length a , and let \mathbf{R} denote the end-to-end vector of a chain. The chain follows a random walk with step length a . The average end-to-end distance is given by

$$(2.9) \quad \langle |\mathbf{R}|^2 \rangle = Na^2 = al, \quad \langle R_i R_j \rangle = \frac{1}{3} \delta_{ij} al, \quad 1 \leq i, j \leq 3,$$

where $l = Na$ is the arc length of the chain, and $\langle \cdot \rangle$ denotes the ensemble average. The probability of a given chain conformation to have an end-to-end vector \mathbf{R} is the Gaussian distribution

$$(2.10) \quad p_N(\mathbf{R}) = \left(\frac{3}{2\pi R_0^2} \right)^{\frac{3}{2}} e^{-\frac{3|\mathbf{R}|^2}{2R_0^2}},$$

characterized by its variance R_0 . Moreover, consistency with (2.9) implies that $R_0^2 = al$. The partition function,

$$Z_N(\mathbf{R}) = p_N(\mathbf{R})Z_N$$

gives the number of configurations with end-to-end vector \mathbf{R} , where Z_N is the total number of chain configurations. So, the free energy of a single chain is

$$(2.11) \quad \mathcal{F} = -k_B T \ln Z_n(\mathbf{R}) = k_B T \left(\frac{3|\mathbf{R}|^2}{2R_0^2} \right) + C,$$

where C is constant.

Another measure of the spatial extension of a single chain is the radius of gyration R_G . It is defined as the root mean square of the distance between each segment of the chain and the center of mass. In the case that the number of segments $N \gg 1$,

$$\langle R_G^2 \rangle \approx \frac{1}{6} N a^2 = \frac{1}{6} al = \frac{1}{6} R_0^2.$$

So, on the average, the shape of a polymer chain at equilibrium is spherical with radius R_G .

The average shape of a liquid crystal polymer is that of an ellipsoid, with step-length tensor L , so that the anisotropic analog of the average of end-to-end distance (2.9) is now

$$(2.12) \quad \langle R_i R_j \rangle = \frac{1}{3} l L_{ij}.$$

Letting l_1, l_2 , and l_3 denote the ellipsoid semiaxes along directions \mathbf{e}_i , $i = 1, 2, 3$, $|\mathbf{e}_i| = 1$, L admits the spectral representation

$$(2.13) \quad L = \sum_{i=1}^3 l_i \mathbf{e}_i \otimes \mathbf{e}_i.$$

We take $l_1 = l_2 := l_\perp$ to represent a uniaxial network giving the spheroidal representation for L , and denote $l_\parallel := l_3$ and $\mathbf{n} := \mathbf{e}_3$, so that

$$(2.14) \quad L = (l_\parallel - l_\perp) \mathbf{n} \otimes \mathbf{n} + l_\perp I.$$

In the prolate symmetry corresponding to main chain polymers, $l_\parallel > l_\perp$, in which case the polymer backbone will stretch along the nematic director \mathbf{n} . (The reverse inequality holds in the case of side-chain oblate elastomers).

The Gaussian distribution of chain conformations generalized to the anisotropic case is

$$(2.15) \quad p_N(\mathbf{R}) = \left[\left(\frac{3}{2\pi l} \right)^3 \frac{1}{\det L} \right]^{\frac{1}{2}} e^{-\frac{3}{2l} (\mathbf{R} \cdot L^{-1} \mathbf{R})}.$$

As in the isotropic case, the affinity property of chain conformations leads to the anisotropic version of the neo-Hookean energy in the form

$$(2.16) \quad \mathcal{W}_{\text{BTW}} = \mu (F \cdot L^{-1} F),$$

where μ denotes the shear modulus. An expression that includes the shape at crosslinking encoded in the initial step-length tensor L_0 is

$$(2.17) \quad \mathcal{W}_{\text{BTW}} = \mu \text{tr}(L_0 F^T L^{-1} F).$$

The latter is the form proposed by Bladon, Warner and Terentjev [41]. In their original work, it is represented in terms of the nematic director \mathbf{n} and the uniaxial order parameter s :

$$(2.18) \quad \begin{aligned} \mathcal{W}_{\text{BTW}} = & \frac{1}{2} \mu \frac{l_{\perp}^0}{l_{\perp}} \left((|F|^2 - (1-r)|F^T \mathbf{n}|^2) \right. \\ & \left. + \left(\frac{1-r_0}{r_0} \right) (|F \mathbf{n}_0|^2 - (1-r)(F^T \mathbf{n} \cdot \mathbf{n}_0)^2) \right), \\ r = & \frac{l_{\perp}}{l_{\parallel}}, \quad r_0 = \frac{l_{\perp}^0}{l_{\parallel}^0}, \end{aligned}$$

as in [41], with \mathbf{n}_0 , l_{\parallel}^0 , and l_{\perp}^0 representing rod alignment and polymer shape, respectively, at crosslinking. From (2.18), we observe that the configuration at crosslinking is also the reference one.

2.2. Material assumptions. Following the property of freely joined rods, we assume that L and Q have common eigenvectors and propose the constitutive relation

$$(2.19) \quad L = a_0 \left(Q + \frac{1}{3} I \right), \quad a_0 > 0,$$

where $a_0 = \text{tr} L$ is constant. The linear constitutive equation (2.19) is analogous to those proposed by Warner and Terentjev [41] and Fried and Sellers [20] stating that, given a symmetric and traceless tensor Q , there is a unique step-length tensor L with trace a_0 .

In order to interpret this condition, and following the approach in [34], we appeal to the spectral representation

$$(2.20) \quad Q = \sum_{i=1}^3 \lambda_i \mathbf{e}_i \otimes \mathbf{e}_i, \quad \lambda_1 + \lambda_2 + \lambda_3 = 0.$$

The eigenvalues of Q satisfy $-\frac{1}{3} \leq \lambda_i \leq \frac{2}{3}$, $i = 1, 2, 3$. For a biaxial nematic, Q admits the representation in terms of the order parameters r and s ,

$$(2.21) \quad Q = r \left(\mathbf{e}_1 \otimes \mathbf{e}_1 - \frac{1}{3} I \right) + s \left(\mathbf{e}_2 \otimes \mathbf{e}_2 - \frac{1}{3} I \right),$$

where

$$s = \lambda_1 - \lambda_3 = 2\lambda_1 + \lambda_2, \quad r = \lambda_2 - \lambda_3 = \lambda_1 + 2\lambda_2.$$

The inequality constraints on λ_i imply restrictions on r and s . Specifically, admissible values of (r, s) belong to the interior of the triangle \mathcal{T} determined by the edges $\partial\mathcal{T}$: $r + s = 1$, $r - 2s = 1$, and $s - 2r = 1$ (Figure 2). It is easy to check that Q reaches its minimum eigenvalue $\lambda = -\frac{1}{3}$ on each edge of $\partial\mathcal{T}$. Hence,

$$(2.22) \quad \det L = 0 \Leftrightarrow \det \left(Q + \frac{1}{3} I \right) = 0 \Leftrightarrow \lambda_{\min}(Q) = -\frac{1}{3} \Leftrightarrow (r, s) \in \partial\mathcal{T}.$$

We finally notice that the uniaxial states correspond to the lines $r = 0$, $s = 0$, and $r = s$. In the latter case, the uniaxial order tensor representation is

$$(2.23) \quad Q = -s \left(\mathbf{n} \otimes \mathbf{n} - \frac{1}{3} I \right), \quad -s \in \left(-\frac{1}{2}, 1 \right), \quad |\mathbf{n}| = 1,$$

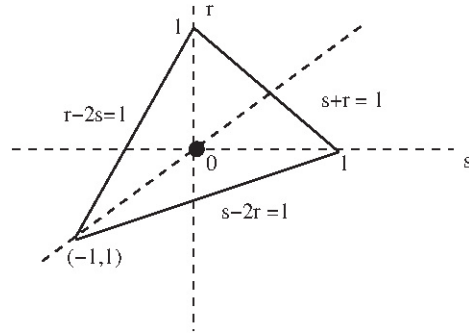


FIG. 2. Q attains the minimum eigenvalue $\lambda = -\frac{1}{3}$ on each one of the edges of the triangle \mathcal{T} . Reproduced from [34].

with $\mathbf{n} := \mathbf{e}_3$ representing the director of the theory. Consistency with (2.13) yields

$$(2.24) \quad a_0 r = (l_1 - l_3), \quad a_0 s = (l_2 - l_3).$$

This reduces to the uniaxial nematic with director \mathbf{n} and order parameter s in the case that

$$l_2 = l_1 := l_\perp, \quad l_3 := l_\parallel.$$

Remark 2. In the uniaxial theory, the order parameter $-s$ in (2.23) is simply denoted as s , a convention that we will follow for the remainder of the article.

2.3. Landau–de Gennes liquid crystal energy. We now examine the energy terms in (2.6), (2.7), and (2.8) involving $|\nabla Q|^2$ and the bulk liquid crystal contribution $f(Q, \xi)$, $\xi > 0$. These are the analogs of a Landau–de Gennes energy density form of a thermotropic liquid crystal,

$$(2.25) \quad \mathcal{W}_{\text{LdG}} = \nu f(Q) + k|\nabla Q|^2,$$

where

$$(2.26) \quad f = a \operatorname{tr}(Q^2) - \frac{b}{3} \operatorname{tr}(Q^3) + \frac{c}{4} (\operatorname{tr} Q^2)^2 + C(a, b, c), \quad a = \frac{\alpha}{2}(T - T_{NI}),$$

$b, c, \alpha > 0$ are material constants, T denotes the absolute temperature, and T_{NI} represents the temperature of transition between the isotropic and nematic phases. The constant $C \geq 0$ guarantees

$$(2.27) \quad f(Q) \geq 0.$$

The function f as in (2.26) has a double-well structure and encodes the phase transition behavior between the nematic and isotropic phases, according to values of the parameter T . In its general form, the second term in (2.25) is a combination of distinctly weighted components of ∇Q [25].

For uniaxial, liquid crystals (2.25) reduces to

$$(2.28) \quad \mathcal{W}_E = k(|\nabla s|^2 + s^2 |\nabla \mathbf{n}|^2) + \nu f(s), \quad s \in \left(-\frac{1}{2}, 1\right).$$

In the case of lyotropic liquid crystals, Kuzuu and Doi ([31] and [32]) assume that f is parametrized by the rod concentration, with high concentration favoring the nematic phase. Moreover, in later work by Ericksen [18], and related applications [8], f is assumed to be a *singular potential* satisfying

$$(2.29) \quad \lim_{s \rightarrow \{-\frac{1}{2}, 1\}} f(s) = +\infty.$$

Remark 3. We point out that the term $k|\nabla Q|^2$ in (2.25) results from simplifying the multiconstant form of the Landau–de Gennes energy [25].

In the current article, we consider the bulk liquid crystal energy densities $f(Q)$, $f(Q, \det F)$, and $\hat{f}(Q, \rho)$. In the latter two functions, the dependence on $\det F$ and ρ , respectively, generalizes that on the concentration parameter of the uniaxial bulk energy density $f(s)$ in (2.28). Indeed, expansion or contraction of the network and changes in rod density have the effect of varying rod concentration. Consequently, statement (2.29) was generalized as follows [33]:

$$(2.30) \quad \lim_{\det(Q + \frac{1}{3}I) \rightarrow 0} f(Q, \xi) = +\infty \text{ for every } \xi > 0.$$

This is equivalent to

$$(2.31) \quad \lim_{\lambda_{\min}(Q) \rightarrow -\frac{1}{3}} f(Q, \xi) = +\infty \text{ for every } \xi > 0.$$

In the case of nematic liquid crystals, the singular limits of $f(Q)$ were stated in [5]. The authors also formulate them in terms of the order parameters as follows: *there exists a smooth function* $\Phi : \mathcal{T} \rightarrow \mathbf{R}^+$ *such that* $f(Q) = \Phi(s, r)$ *and*

$$(2.32) \quad \lim_{(s,r) \rightarrow \partial\mathcal{T}} \Phi(s, r) = +\infty.$$

Remark 4. Finally, we point out the regularizing role of the term $|\nabla Q|^2$ in the Landau–de Gennes elastomer energies (2.6), (2.7), and (2.8). Using the Onsager theory of rigid rods, and assuming either the Lennard–Jones or a hard core interaction potential ([26] and [30]), the material constants k and ν are found to satisfy the relation $\nu = O(\frac{k}{L_a^2})$. For the systems that we consider, typical values of the rod length L_a are in the range from 10^{-9} to 10^{-6} m, rendering the gradient term a small perturbation of the energy.

3. Energy minimization. We present and analyze several variational problems associated with the energy functionals (2.6) and (2.8). The motivations leading to the choice of such problems are multifold. First of all, we pay special attention to the incompressible elastomer since it is a valid model for anisotropic rubbers. Within this class, we consider two distinctive bulk liquid crystal energy density functions, corresponding to $f(Q)$ being a polynomial (2.26), and to the case that it is a singular potential as in (2.31) (with $\det F = 1$). The first case, although it will require a restriction on the class of admissible fields Q , is abundantly justified since the vast majority of works found in the physics literature assume the polynomial form (2.26). Two main reasons call for the analysis of the compressible elastomer. First of all, it offers the appropriate setting for the mathematical treatment of gels, and second, it is appropriate for the case when rod density is a main variable field of the problem, such

as in the study of actin filament networks. Auxiliary results that enter the proofs of the forthcoming theorems are set in the appendix.

Remark 5. The results that follow hold for any prescribed $L_0 \in \mathbb{S}_+^3$ in the definition (2.2). However, to simplify the presentation, we develop the proofs for the case $L_0 = I$.

We start with making the following assumption s on $\hat{W}(G)$ motivated by the analogous ones in isotropic nonlinear elasticity [4].

Polyconvexity: there exists a convex function $\Psi : \mathbb{M}_+^3 \times \mathbb{M}_+^3 \times (0, \infty) \rightarrow \mathbb{R}$ such that \hat{W} in (2.6) and (2.8) satisfies

$$(3.1) \quad \hat{W}(G) = \Psi(G, \text{adj } G, \det G).$$

Coerciveness: there exist constants α, β, p, q, r such that

$$(3.2) \quad \begin{aligned} \alpha > 0, p \geq 2, q \geq \frac{p}{p-1}, r > 1, \\ \hat{W}(G) \geq \alpha(|G|^p + |\text{adj } G|^q + (\det G)^r) + \beta \\ \text{for almost all } \mathbf{X} \in \Omega \text{ and for all } F \in \mathbb{M}_+^3. \end{aligned}$$

Moreover, in the case that the elastomer is compressible, we also require

Growth near zero determinant:

$$(3.3) \quad \lim_{\det G \rightarrow 0^+} \hat{W}(G) = +\infty.$$

Remark 6. The assumption $p \geq 2$ has deep consequences on the nature of the energy minimizers established in this section. It is well known that for $2 \geq p \geq 3$ and in three space dimensions, injectivity of the deformation map $\mathbf{x} = \boldsymbol{\varphi}(\mathbf{X})$ is not guaranteed and, therefore, the Lagrangian tensors $Q(\mathbf{X})$, $L(\mathbf{X})$, and the scalar $\rho(\mathbf{X})$ may not admit Eulerian counterparts, defined in $\boldsymbol{\varphi}(\Omega)$. These can be addressed by two approaches. The first one consists in imposing the more restrictive assumption $p > 3$ in (3.2) and Dirichlet boundary data on the boundary (or part of it). However, this is not quite a desirable outcome, since the resulting class of elastomer energies do not involve the neo-Hookean form by Bladon, Warner, and Terentjev. In the second approach, we maintain $p \geq 2$ but we add a new energy term in (2.6) and (2.8). This term penalizes the surface created around cavities and boundary contact points, both resulting from possible loss of injectivity [27]. (This is the subject of current work by the authors.)

Remark 7. The following statement is a straightforward consequence of (2.2), (2.19), and (2.22):

$$(3.4) \quad \det G \rightarrow 0^+ \iff \det F \rightarrow 0^+ \text{ provided } \lambda_{\min}(Q) > -\frac{1}{3} + \epsilon$$

for some $\epsilon > 0$.

Remark 8. We observe that the condition on the exponents p and q of (3.2) guarantees $\frac{1}{p} + \frac{1}{q} < \frac{4}{3}$. This is a required condition to obtain convergence of weak limits of sequences of determinants in the proof of existence of a minimizer (Theorem 3.1).

We impose Dirichlet boundary conditions on $\Gamma_0 \subseteq \partial\Omega$. Let $\hat{\boldsymbol{\varphi}} \in H^{\frac{1}{2}}(\Gamma_0, \mathbb{R}^3)$ be injective and $\hat{Q} \in H^{\frac{1}{2}}(\Gamma_0, \mathbb{S}_0^3)$ be prescribed and such that

$$(3.5) \quad \boldsymbol{\varphi}(\mathbf{X}) = \hat{\boldsymbol{\varphi}}(\mathbf{X}) \quad \text{and} \quad Q(\mathbf{X}) = \hat{Q}(\mathbf{X}), \quad \mathbf{X} \in \Gamma_0.$$

The following theorem is a special case of [4, Theorem 6.2]. We will apply it in the proofs of the existence of minimizer of the total energy, as in the case of isotropic elasticity.

THEOREM 3.1. *Suppose that $\Omega \subset \mathbb{R}^n$ is open.*

- $n = 3$: *If $u_r \rightharpoonup u$ in $W^{1,p}(\Omega)$ and $\text{adj } \nabla u_r \rightharpoonup \text{adj } \nabla u$ in L^q with $p > 1$, $q > 1$, and $\frac{1}{p} + \frac{1}{q} < \frac{4}{3}$, then $\det \nabla u_r \rightarrow \det \nabla u$ in $\mathcal{D}'(\Omega)$.*
- $n = 2$: *If $u_r \rightharpoonup u$ in $W^{1,p}(\Omega)$ and $p > \frac{4}{3}$ then $\det \nabla u_r \rightarrow \det \nabla u$ in $\mathcal{D}'(\Omega)$.*

3.1. Incompressible Landau–de Gennes elastomer. In this section, we prove existence of an energy minimizer for two different forms of the liquid crystal bulk energy $f(Q)$. We first consider the case that $f(Q)$ is the standard Landau–de Gennes polynomial and in our second approach, we assume that the function $f(Q)$ is defined as in (2.30) and (2.32).

3.1.1. Restriction on the domain of Q . We now include a new constraint on the elements $Q \in \mathbb{S}_0^3$ of the admissible set: for a given $\varepsilon > 0$, $\lambda_{\min}(Q) \geq -\frac{1}{3} + \varepsilon$. We note that even the strict bound $\lambda_{\min}(Q) > -\frac{1}{3}$ is not sufficient to guarantee that the limit Q^* of the minimizing sequences $\{Q_k\}$ satisfies the same strict lower bound so as to guarantee the invertibility of L obtained from (2.19).

As in [10], we define the set

$$(3.6) \quad \mathcal{Q}(a) = \{Q \in \mathbb{S}_0^3, \lambda_{\min}(Q) \geq a\},$$

where a is some real number, and define $\mathcal{Q}_\varepsilon = \mathcal{Q}(-1/3 + \varepsilon)$, where $0 < \varepsilon \leq 1/3$ is an arbitrary constant.

PROPOSITION 3.2. *The set $\mathcal{Q}(a)$ is convex in \mathbb{S}_0^3 .*

Proof. Take any two matrices Q_1 and Q_2 in $\mathcal{Q}(a)$, and let

$$Q = \alpha_1 Q_1 + \alpha_2 Q_2,$$

where $\alpha_i \geq 0, i = 1, 2$, and $\alpha_1 + \alpha_2 = 1$. Since $Q \in \mathbb{S}_0^3$, we only need to show that $\lambda_{\min}(Q) \geq a$. By Rayleigh's formula, we have

$$\begin{aligned} \lambda_{\min}(Q) &= \min_{|\mathbf{x}|=1} \mathbf{x}^T Q \mathbf{x} = \min_{|\mathbf{x}|=1} \left(\sum_{i=1}^2 \alpha_i \mathbf{x}^T Q_i \mathbf{x} \right) \\ &\geq \sum_{i=1}^2 \alpha_i \min_{|\mathbf{x}|=1} \mathbf{x}^T Q_i \mathbf{x} = a. \end{aligned}$$

Hence $Q \in \mathcal{Q}(a)$ and so the convexity of $\mathcal{Q}(a)$ follows. \square

For any matrix $Q \in \mathbb{S}_0^3$, since $\text{tr}(Q) = 0$, $\lambda_{\min}(Q) \leq 0$ and $\lambda_{\max}(Q) \geq 0$ hold. The following proposition gives a bound on $\lambda_{\max}(Q)$ based on $\lambda_{\min}(Q)$.

PROPOSITION 3.3. *Let $Q \in \mathbb{S}_0^3$. Then*

$$(3.7) \quad \lambda_{\max}(Q) \leq -2\lambda_{\min}(Q).$$

Proof. For any matrix Q in \mathbb{S}_0^3 , let its eigenvalues satisfy $\lambda_1 \leq \lambda_2 \leq \lambda_3$. Since $\text{tr}(Q) = \lambda_1 + \lambda_2 + \lambda_3 = 0$, we have

$$-\lambda_3 = \lambda_1 + \lambda_2 \geq 2\lambda_1.$$

The conclusion follows by multiplying both sides of the previous inequality by -1 . \square

Now we turn to the questions of estimating eigenvalues of L and L_0 given by (2.19) for $Q, Q_0 \in \mathcal{Q}_\varepsilon$. Note that L and L_0 are both symmetric and positive definite, so that the anisotropic deformation tensor G in (2.2) is well defined. By Proposition 3.3, we have that

$$\lambda_{\max}(Q) \leq -2\lambda_{\min}(Q) \leq \frac{2}{3} - 2\varepsilon.$$

So, using the constitutive relation (2.19) gives

$$(3.8) \quad \lambda_{\max}(L) \leq a_0(1 - 2\varepsilon) \leq a_0.$$

Moreover, since $\lambda_{\min}(Q_0) \geq -\frac{1}{3} + \varepsilon$, using again (2.19) yields

$$(3.9) \quad \lambda_{\min}(L_0) \geq a_0\varepsilon.$$

Hence, from Lemma 6.3, we have that

$$(3.10) \quad |G| \geq \sqrt{\varepsilon}|F| \quad \text{and}$$

$$(3.11) \quad |\text{adj}(G)| \geq \frac{1}{3}\varepsilon|\text{adj}(F)|.$$

Let $\varepsilon > 0$ and consider the problem of minimizing (2.6) on the admissible set

$$(3.12) \quad \mathcal{A}_\varepsilon = \{\varphi \in W^{1,p}(\Omega, \mathbb{R}^3), Q \in W^{1,2}(\Omega, \mathcal{Q}_\varepsilon) : \text{adj}(\nabla\varphi) \in L^q(\Omega, \mathbb{M}^3), \\ \det \nabla\varphi = 1 \text{ a.e., and (3.5) holds}\}$$

with p and q as in (3.2). The following theorem proves existence of a global minimizer of the energy.

THEOREM 3.4. *Let $\Omega \in \mathbb{R}^3$ be open and bounded, with smooth boundary $\partial\Omega$, and let $\Gamma_0 \subseteq \partial\Omega$ be as in (3.5). Let the total energy be as in (2.7) and suppose that relations (2.2) and (2.19) hold. Assume that hypotheses (2.26), (3.1), and (3.2) hold. Then, there exists at least one pair $(\varphi^*, Q^*) \in \mathcal{A}_\varepsilon$ such that*

$$(3.13) \quad \mathcal{E}(\varphi^*, Q^*) = \inf_{(\varphi, Q) \in \mathcal{A}_\varepsilon} \mathcal{E}(\varphi, Q).$$

Proof. First of all, we point out that the integrals in the definition of \mathcal{E} are well defined. We observe as well that $\mathcal{A}_\varepsilon \neq \emptyset$ and therefore, there exists a constant $K_1 > 0$ such that the following inequality holds:

$$(3.14) \quad \inf_{(\varphi, Q) \in \mathcal{A}_\varepsilon} \mathcal{E} < K_1.$$

Step 1. Coercivity. From the coercivity hypothesis (3.2) on $\hat{W}(G)$ and property (2.27), it follows that

$$(3.15) \quad \mathcal{E}(\varphi, Q) \geq \alpha \int_{\Omega} (|G|^p + |\text{adj} G|^q + |\nabla Q|^2) d\mathbf{X}.$$

Likewise, the positivity of $\hat{W}(G)$ implies that

$$(3.16) \quad \mathcal{E}(\varphi, Q) \geq \int_{\Omega} f(Q) d\mathbf{X}.$$

According to the generalized Poincaré inequality [12, p. 281], there exists a constant $c > 0$ such that

$$(3.17) \quad \int_{\Omega} |\varphi|^p d\mathbf{X} \leq c \left\{ \int_{\Omega} |\nabla \varphi|^p d\mathbf{X} + \left| \int_{\Gamma_0} \varphi dS \right|^p \right\}$$

for all $\varphi \in W^{1,p}(\Omega)$. Likewise,

$$(3.18) \quad \int_{\Omega} |Q|^2 d\mathbf{X} \leq c \left\{ \int_{\Omega} |\nabla Q|^2 d\mathbf{X} + \left| \int_{\Gamma_0} Q dS \right|^2 \right\}.$$

Now, combining (3.10), (3.11), (3.17), and (3.18) with the fact that $p \geq 2$ gives the existence of constants $C > 0$ and c_0 such that

$$(3.19) \quad \mathcal{E}(\varphi, Q) \geq C \|\varphi\|_{1,p}^p + \|\text{adj } F\|_{0,q}^q + \|Q\|_{1,2}^2 - c_0.$$

The latter inequality guarantees the existence of a constant K_0 , which together with (3.14) yields

$$(3.20) \quad K_0 < \inf_{(\varphi, Q) \in \mathcal{A}_\varepsilon} \mathcal{E} < K_1.$$

Let $(\varphi_k, Q_k) \in \mathcal{A}_\varepsilon$ be a minimizing sequence for \mathcal{E} , that is,

$$(3.21) \quad \lim_{k \rightarrow \infty} \mathcal{E}(\varphi_k, Q_k) = \inf_{(\varphi, Q) \in \mathcal{A}_\varepsilon} \mathcal{E}.$$

Step 2. Compactness. From inequality (3.19), it follows that

$$\mathcal{E}(\varphi_k, Q_k) \rightarrow \infty, \text{ as } (\|\varphi_k\|_{1,p} + \|\text{adj } F_k\|_{0,q} + \|Q_k\|_{1,2}) \rightarrow \infty,$$

which together with the second inequality in (3.20) implies that

$$(\varphi_k, \text{adj } \nabla \varphi_k, Q_k) \text{ is bounded in the reflexive Banach space } W^{1,p} \times L^q \times W^{1,2}.$$

Therefore there exist weakly convergent subsequences such that

$$(3.22) \quad \varphi_k \rightharpoonup \varphi^* \text{ in } W^{1,p},$$

$$(3.23) \quad \text{adj } \nabla \varphi_k \rightharpoonup H^* \text{ in } L^q,$$

$$(3.24) \quad Q_k \rightharpoonup Q^* \text{ in } W^{1,2}.$$

Step 3. Properties of φ^ and Q^* .* From (3.22) and (3.23), we have by Theorem 3.1 that

$$(3.25) \quad \begin{aligned} H^* &= \text{adj}(\nabla \varphi^*) \quad \text{and} \\ \det(\nabla \varphi^*) &= \det(\nabla \varphi_k) = 1 \quad \text{a.e. in } \Omega. \end{aligned}$$

Also, by Proposition 3.2 and Mazur's theorem, the set $\{Q \in H^1(\Omega, \mathbb{M}^3) : Q \in \mathcal{Q}_\varepsilon \text{ a.e. in } \Omega\}$ is weakly closed. Thus it follows from (3.24) that $Q^* \in \mathcal{Q}_\varepsilon$ a.e. in Ω . Hence $(\varphi^*, Q^*) \in \mathcal{A}_\varepsilon$.

Finally, the existence of a minimizer follows from the lower semicontinuity of \mathcal{E} , due to the polyconvexity assumption on $\hat{W}(G)$ and the continuity of f . This concludes the proof of the theorem. \square

Remark 9. Note that the previous result applies to the Bladon–Terentjev–Warner energy only in the case $n = 2$. This is a direct consequence of Theorem 3.1.

3.1.2. Nonpolynomial growth of the bulk energy $f(Q)$: Case of singular potential. We now study the case that $f(Q)$ is a singular potential that blows up at the limit $\det(Q + \frac{1}{3}I) = 0$. Let \mathcal{Q}_0^+ be as in (1.2) and define the following admissible set:

$$(3.26) \quad \mathcal{A}_0 = \{ \varphi \in W^{1,p}(\Omega, \mathbb{R}^3), Q \in W^{1,2}(\Omega, \mathcal{Q}_0^+) : \text{adj}(\nabla\varphi) \in L^q(\Omega, \mathbb{M}^3), \det \nabla\varphi = 1 \text{ a.e.}, \text{ and (3.5) holds.} \}$$

THEOREM 3.5. *Let Ω and Γ_0 be as in Theorem 3.4 and suppose that relations (2.2) and (2.19) hold. Assume that hypotheses (3.1) and (3.2) hold, and that the bulk energy density satisfies $\lim_{\lambda_{\min}(Q) \rightarrow -\frac{1}{3}} f(Q) = +\infty$. Suppose that the prescribed boundary tensor has the property $\lambda_{\min}(\hat{Q}) > -\frac{1}{3} + \varepsilon$ for some $\varepsilon > 0$. Then the total energy (2.7) has a global minimizer in (3.26).*

Proof. It is easy to see that Steps 1 and 2 of the proof of the previous theorem follow as well in this case. Let $\{(\varphi_k, Q_k)\}_{k \geq 1}$ denote a minimizing sequence of the energy in \mathcal{A}_0 .

Step 3. Properties of φ^ and Q^* .* First of all, we note that (3.25) also holds in this case. We now study properties of the minimizing sequence $\{Q_k\}$ to show that $Q^* \in \mathcal{Q}_0^+$. We first observe that the strong convergence of $\{Q_k\}$ to Q^* in L^2 follows from (3.24), and, up to a subsequence, it implies that

$$(3.27) \quad Q_k \rightarrow Q^* \text{ a.e. in } \Omega.$$

Let $q^m := \det(Q_m + \frac{1}{3}I)$ and note that

$$q^m > 0 \text{ a.e. in } \Omega \Leftrightarrow q^* \geq 0 \text{ a.e. in } \Omega.$$

We want to prove that $q^* > 0$ a.e. in Ω . For this, suppose that $q^* = 0$ on a set $A \subset \Omega$, $\text{vol}(A) > 0$. Since $0 < d^l \rightarrow d^*$, we have

$$\int_A \left| \det \left(Q^l + \frac{1}{3}I \right) \right| d\mathbf{X} = \int_A \det \left(Q^l + \frac{1}{3}I \right) d\mathbf{X} \rightarrow \int_A \det \left(Q^* + \frac{1}{3}I \right) d\mathbf{X} = 0.$$

We now consider the sequence $f^m := f(Q^m)$ of measurable functions of \mathbf{X} . Since $f^m \geq 0$, by Fatou's theorem

$$\int_A \liminf_{m \rightarrow \infty} f^m(\mathbf{X}) d\mathbf{X} \leq \liminf_{m \rightarrow \infty} \int_A f^m(\mathbf{X}) d\mathbf{X}.$$

By the growth assumption (2.32) on f

$$\liminf_{m \rightarrow \infty} f^m = \lim_{\det(Q + \frac{1}{3}I) \rightarrow 0} f(Q) = +\infty,$$

and consequently $\lim_{m \rightarrow \infty} \int_A f(Q^m(x)) d\mathbf{X} = +\infty$. But the latter relation contradicts the statement that $\int_{\Omega} f(Q_k) < K_1$ that follows from (3.16). Hence $Q^* \in \mathcal{Q}_0^+$ a.e. in Ω .

Finally, existence of an energy minimizer in \mathcal{A}_0 follows from the polyconvexity of \hat{W} , the weak lower semicontinuity of $\int_{\Omega} f$ that follows from Fatou's theorem, and the fact that the pair (φ^*, Q^*) satisfies the boundary conditions prescribed to the elements of \mathcal{A}_0 . The latter is a consequence of the compactness of the trace operator mapping $W^{1,p}(\Omega)$ to $L^p(\Omega)$ (and the analogous one for the tensor Q). \square

3.2. Compressible Landau–de Gennes elastomer. In this section, we study minimization of the energy functional (2.6). In addition to (2.30), we also assume that

$$(3.28) \quad \lim_{\det F \rightarrow (0, \infty)} f(Q, \det F) = +\infty \quad \text{for each } Q \in \mathcal{S}_0^3.$$

This condition penalizes deformations with extreme volume change and it is similar to (2.2) on the elastic energy. The admissible set is

$$(3.29) \quad \mathcal{A}_C = \{ \varphi \in W^{1,p}(\Omega, \mathbb{R}^3), Q \in W^{1,2}(\Omega, \mathcal{Q}_0) : \text{adj } G \in L^q(\Omega, \mathbb{M}^3), \\ \det G \in L^r(\Omega, \mathbb{R}^+), \det \nabla \varphi > 0 \text{ a.e., and (3.5) holds} \}.$$

THEOREM 3.6. *Let Ω and Γ_0 be as in Theorem 3.4 and suppose that relations (2.2) and (2.19) hold. Suppose that the free energy density is as in (2.6). Assume that (3.1), (3.2), (2.30), (3.3), and (3.28) are satisfied. Moreover, we require that one of the following holds:*

1. *if f in (2.6) is convex with respect to $\det F$, we take $g \equiv 0$;*
2. *if f is nonconvex, we assume that $g \geq 0$ and not identically 0 is a smooth and convex function.*

Then the total energy admits a minimizer in \mathcal{A}_C .

Proof. We observe that Steps 1 and 2 of the proof of Theorem 3.4 apply to this case as well. We need to establish that (φ^*, Q^*) belong to the admissible set by showing that $\det \nabla \varphi^* > 0$. If $g \neq 0$, it follows by Fatou's theorem along the same lines of the proof of $\det \nabla \varphi^* = 1$ in the incompressible case. If $g \equiv 0$, the proof can also be given using Mazur's theorem on f . Existence of a minimizer follows from the polyconvexity of \hat{W} together with Fatou's theorem that provides the weak lower semicontinuity of f and g . \square

Remark 10. The energy minimizer may not be uniaxial even in the case that L_0 and \hat{Q} are uniaxial. In fact, the same statement is true for the minimizer of the Landau–de Gennes energy of the pure liquid crystal problem [34]. In that case, numerical results give strong evidence of uniaxiality when \hat{Q} is uniaxial.

Remark 11. The two sets of assumptions on f and g are meant to deal with the convexity properties of $f(\det F, Q)$ with respect to $\det F$. Convexity of f is sufficient to provide information on the weak limits of sequences of determinants. However, nonconvexity occurs when phase transitions are involved, in which case g has the role of controlling the determinant.

3.2.1. Rod fluids with elastic crosslinks. We now analyze a model for the elastically interacting nematic units motivated by models of actin networks. We assume that the total energy is as in (2.8).

Let $\hat{\varphi}$ and \hat{Q} be as in (3.5) and $\hat{\rho} \in H^{\frac{1}{2}}(\Gamma_0, \mathbb{R}^+)$. We assume that

$$(3.30) \quad \hat{f} \in C(\mathcal{S}_0^3 \times (0, \infty), \mathbb{R}^+),$$

$$(3.31) \quad g \geq 0 \text{ is smooth and convex,}$$

$$(3.32) \quad \lim_{\rho \rightarrow \{0, \infty\}} \hat{f}(Q, \rho) = +\infty \text{ for each } Q \in \mathcal{S}_0^3,$$

$$(3.33) \quad \lim_{\det(Q + \frac{1}{3}I) \rightarrow 0} \hat{f}(Q, \rho) = +\infty \text{ for each } \rho \in (0, \infty).$$

We let $\rho_0 > 0$ denote the prescribed reference rod density and assume that the equation of balance of mass

$$(3.34) \quad \rho(\mathbf{X}) \det(\nabla \varphi)(\mathbf{X}) = \rho_0, \quad \mathbf{X} \in \Omega \text{ a.e.}$$

of rods holds. We define the admissible set as

$$(3.35) \quad \begin{aligned} \mathcal{A}_\rho = \{ & \varphi \in W^{1,p}(\Omega, \mathbb{R}^3), Q \in W^{1,2}(\Omega, \mathcal{Q}_0^+) : \text{adj } G \in L^q(\Omega, \mathbb{M}^3), \\ & \det G \in L^r(\Omega, \mathbb{R}^+), \rho \in W^{1,2}(0, \infty), \rho > 0 \text{ a.e.}, (3.34) \text{ holds,} \\ & \rho = \hat{\rho}, \varphi = \hat{\varphi}, \text{ and } Q = \hat{Q} \text{ on } \Gamma_0 \}. \end{aligned}$$

We now formulate the main theorem of existence of a minimizer for the rod system.

THEOREM 3.7. *Let Ω and Γ_0 be as in Theorem 3.4 and suppose that relations (2.2) and (2.19) hold. Suppose that the free energy density is as in (2.8) with $g \equiv 0$. Suppose that the assumptions (3.1), (3.2), (3.3), (3.30), (3.32), and (3.33) are satisfied. Then the total energy admits a minimizer in \mathcal{A}_ρ .*

Proof. Once more, Steps 1 and 2 of the proof follow as in Theorem 3.4. This yields sequences $\{\phi_k, Q_k\}$ with properties (3.22), (3.23), (3.24). Moreover, it follows from Theorem 3.1 that $\det \nabla \varphi_k \rightarrow \det \nabla \varphi^* > 0$ in $D'(\Omega)$.

Let $\{\rho_k\}$ denote the minimizing sequence corresponding to the rod density. It is easy to see that the analog of relations (3.20) and (3.19) now yield

$$(3.36) \quad \int_{\Omega} |\nabla \rho_k|^2 d\mathbf{X} < K.$$

This, together with Poincaré's inequality yields a subsequence such that $\rho_k \rightarrow \rho^*$ in $L^2(\Omega)$ and $\rho_k \rightarrow \rho^*$ a.e. in Ω . The a.e. convergence of $\{\rho_k\}$ to ρ^* and the convergence of the sequence of determinants yield

$$\rho_0 = \rho_k \det \nabla \varphi_k \rightarrow \rho^* \det \nabla \varphi^*.$$

Hence the balance of mass equation (3.34) is satisfied at the limit. The verification that the limiting fields satisfy the boundary conditions in (3.35) follow as in Theorem 3.4. \square

Finally, we state the theorem of existence of a minimizer in the case that Φ in (3.1) is independent of $\text{adj } F$ and $\det F$, that is, the elastomer free energy density function is that of a Hadamard material [12]. In this case, we set the admissible set as

$$\begin{aligned} \mathcal{A}_H = \{ & \varphi \in W^{1,p}(\Omega, \mathbb{R}^3), Q \in W^{1,2}(\Omega, \mathcal{Q}_0^+), \rho \in W^{1,2}(0, \infty), \\ & \rho > 0 \text{ a.e. in } \Omega, (3.34) \text{ holds, } \rho = \hat{\rho}, \varphi = \hat{\varphi}, \text{ and } Q = \hat{Q} \text{ on } \Gamma_0 \}. \end{aligned}$$

The proof of the next theorem follows as that of Theorem 3.7, where now the convergence of the sequence of determinants and the positivity of the limit determinant follow from the convexity of g .

THEOREM 3.8. *Let Ω and Γ_0 be as in Theorem 3.4 and suppose that relations 2.2 and 2.19 hold. Suppose that the free energy density in (2.8) is such that $\hat{W}(G) = \Psi(|G|) \geq 0$, with $\Psi(\cdot)$ smooth and convex and let $g \neq 0$ satisfy (3.31). Suppose that the assumptions (3.30), (3.32), and (3.33) are satisfied. Then the total energy admits a minimizer in \mathcal{A}_H .*

4. Liquid crystal phase transitions in actin networks. In this section, we apply the energy functions (2.8) to model density dependent liquid crystal phase transitions in actin networks. These are a class of cytoskeletal networks consisting of stiff actin rods jointed by flexible crosslinkers. Their properties emerge from the interaction of liquid rod behavior and network elasticity.

Parameters to characterize these networks include the ratio $\chi = L_a/L_x^0$ of the typical lengths L_a of the actin rod and that of the the crosslinker, L_x^0 , in the reference

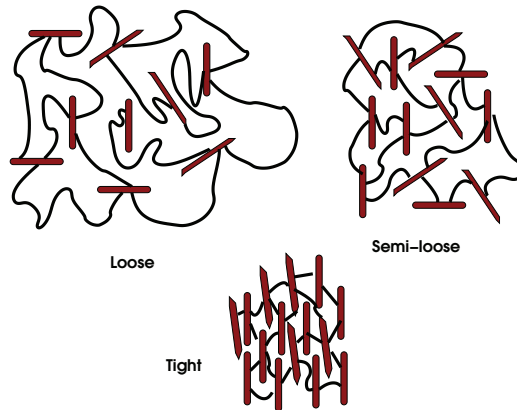


FIG. 3. Three types of actin network according to χ . Reproduced from [14].

configuration, the rod aspect ratio A_a , the rod reference density ρ_0 , and the reference crosslink density σ_x^0 . These are also the reference parameters used in the Monte Carlo simulations of these systems by Bates and Frenkel [6] (rigid rod fluids) and Dalhaimer, Discher, and Lubensky [14] (crosslinked rigid rod networks). These works together with the studies of lyotropic liquid crystals by Kuzuu and Doi [31] motivate the constitutive assumptions in our continuum mechanics treatment. We assume that the molecular interactions responsible for nematic phases in rodlike fluids compete with the solidlike elastic forces due to network crosslinking. We formulate this assumption in terms of the relative energy scales of fluid and solid systems. Our goal is to adopt the simplest possible set of assumptions capable of explaining the phase transition behavior.

In [14], the authors argued that the actin network can be classified into three regimes according to values of the ratio $\chi = L_a/L_x^0$, where L_a is the length of the actin fiber, and L_x^0 is the typical length of the crosslinker in the reference configuration, as shown in Figure 3. They found that

- when $\chi < \chi_l$, the network is isotropic in the stress-free state (external force $\Sigma = 0$) or under expansion ($\Sigma > 0$), and the network will become nematic under large enough compression ($\Sigma \leq \Sigma_c < 0$);
- when $\chi_l < \chi < \chi_r$, the network is nematic in the stress-free state (external force $\Sigma = 0$), or under compression ($\Sigma < 0$), and the network will become isotropic under large enough expansion ($\Sigma \geq \Sigma_c > 0$);
- when $\chi > \chi_r$, the network is nematic regardless of the type of applied force.

4.1. Parameters of the model and assumptions. We assume that the system is characterized by

1. the reference configuration $\Omega \subset \mathbf{R}^3$ and the previously defined positive quantities L_x^0 , ρ_0 , σ_x^0 , χ , and A_a ;
2. the energy scaling parameters

$$(4.1) \quad \mu = RT\sigma_x^0, \quad \nu = RTA_a\rho_0,$$

where R is the gas constant and T the absolute temperature. In particular, they reflect the property that an increase in the rod aspect ratio, while holding the other parameters fixed, tends to favor nematic equilibrium.

Remark 12. Since the rods are not randomly located in space as in the case of a fluid but serve as crosslink sites, ρ_0 and L_x^0 are not independent. For systems such that $L_x^0 \gg L_a$, the following estimate holds:

$$(4.2) \quad \rho_0 = \frac{\text{total volume of rods}}{\text{total undeformed volume}} = K \frac{\chi^3}{\mathcal{A}_a^2}.$$

We have taken the material of the rod as having mass density 1. K is a network constant that accounts for the number of crosslinks per actin unit and the coordination number of the network. Moreover, in estimating the denominator, we have assumed that the total volume of the system is fully spanned by the network.

Physiological values for the model parameters are available in the literature. In the case of cochlear outer hair cells the diameter of a typical actin filament varies from 5 to 8 nm. The maximum reported length is 1 μm [28, 7]. Data for the linkers length is also available; for this type of material, lengths vary in the range from 50 nm to 260 nm. With these values we estimate model parameters like χ and the aspect ratio A_a . In particular, typical values of χ can be found in the range from 3.8 to 20.

4.1.1. Nematic rod fluid. We assume that $f : (-\frac{1}{2}, 1) \times (0, \infty) \rightarrow \mathbf{R}$ represents a uniaxial bulk energy, parametrized by $\chi > 0$, so that the following hold.

1. There exists a critical value χ_t such that, for $0 < \chi < \chi_t$, f has two local minima $\{s = 0, \rho = \rho_0\}$ and $\{s^* > 0, \rho^* > \rho_0\}$. For $\chi > \chi_t$, only the nematic minimum remains.
2. There exists a critical value $\chi_l < \chi_t$ such that,

$$(4.3) \quad f(0, \rho_0; \chi) < f(s^*, \rho^*; \chi) \quad \text{for } 0 < \chi < \chi_l,$$

$$(4.4) \quad f(0, \rho_0; \chi) > f(s^*, \rho^*; \chi) \quad \text{for } \chi_l < \chi < \chi_t,$$

$$(4.5) \quad f(0, \rho_0; \chi_l) = f(s^*, \rho^*; \chi_l).$$

3. $f(s^*, \rho^*; \chi)$ decreases with increasing χ , and s^* increases and ρ^* decreases, also with respect to χ .
4. f has a maximum at $s = s^{**}, \rho = \rho^{**}, 0 < s^{**} < s^*, \rho_0 < \rho^{**} < \rho^*$.
5. It satisfies growth conditions with respect to s and ρ :

$$(4.6) \quad \lim_{s \rightarrow \{-\frac{1}{2}, 1\}} f(s, \rho; \chi) = +\infty \text{ for all } \rho > 0,$$

$$(4.7) \quad \lim_{\rho \rightarrow \{0, \infty\}} f(s, \rho; \chi) = +\infty \text{ for all } s \in \left(-\frac{1}{2}, 1\right).$$

An example of a function satisfying the proposed growth conditions is presented in Figure 4. In the next section, we provide a method of constructing a function f satisfying these properties.

4.2. Density dependent phase transitions. Let us consider deformations with gradient

$$(4.8) \quad F = \text{diag}(\lambda, \lambda, \lambda), \quad \rho \lambda^3 = \rho_0.$$

Set $\mathbf{n}_0 = 0$, choose $W = \mathcal{W}_{\text{BTW}}$ as in (2.18), and calculate the total energy density

$$(4.9) \quad \mathcal{E} := \lambda^3 (\mu(1 - \alpha s^2) + \nu f(s, \rho; \chi)).$$

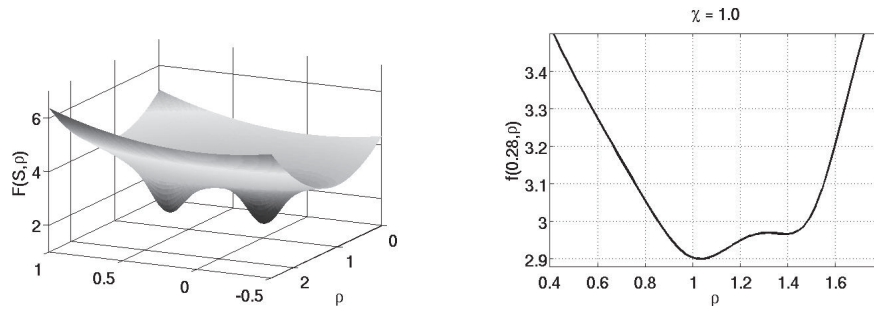


FIG. 4. 3D plot of the bulk free energy (left) and its corresponding cross section at $s = 0.28$ (right) in the case $\chi = 1.0$.

We consider \mathcal{E} parametrized by ρ and calculate the critical points

$$(4.10) \quad \frac{d\mathcal{E}}{ds} = \lambda^3 (-2\alpha\mu s + \nu f_s(s, \rho; \chi)) = 0.$$

We now discuss the solvability of the critical point equation as the parameter ρ varies. In the case of multiple solutions, we choose that with the lowest energy. We summarize the results as follows.

PROPOSITION 4.1. *Let $\rho_0 > 0$ be prescribed. Then the homogeneous minimizers of the energy have the following properties:*

1. for $\chi \geq \chi_t$, the minimizer $s = s(\rho, A_a, \chi) > 0$ for all $\rho > 0$ with $s(\rho, A_a, \cdot)$ increasing and such that $s(\rho, A_a, \chi) \rightarrow 1$ as $\chi \rightarrow \infty$;
2. for $0 \leq \chi \leq \chi_t$, there exists a function $\rho = R(A_a, \chi)$, decreasing as A_a increases, with χ held fixed, and increasing as χ decreases, with A_a held fixed, and such that the minimizers satisfy

$$(4.11) \quad s(\rho, A_a, \chi) > 0 \text{ for } \rho \geq R(A_a, \chi),$$

$$(4.12) \quad s(\rho, A_a, \chi) \approx 0 \text{ for } \rho < R(A_a, \chi).$$

Moreover, $R(A_a, \chi) \rightarrow \infty$ as $\chi \rightarrow 0$. Furthermore, $s(\cdot, A_a, \chi)$ may be discontinuous across $R(\cdot)$.

Comparing the liquid crystal behavior of the system under expansion with the next simulations on extension provides additional information on network effects.

4.2.1. Isotropic-nematic phase transitions. We now carry out numerical simulations to describe the phase transition behavior under plane strain deformation given by

$$(4.13) \quad F = \text{diag}(\lambda, \lambda, 1), \quad \lambda^2 \rho = \rho_0.$$

We present three types of plots: the phase diagrams (Figures 5 and 6) in the (ρ, A_a) -plane, the equilibrium order parameter s in terms of the extension ratio λ (Figures 7 and 8), and the stress-strain diagrams (Figure 9).

The phase diagrams are obtained by solving the equation of critical points, that is, the analog of (4.10) and, in the case of multiple solutions, plotting that with smallest energy. Specifically, let us define, the *isotropic* $\mathcal{E}_{iso} = \mathcal{E}(s = 0, \rho)$ and the *nematic* $\mathcal{E}_{nema} = \mathcal{E}(s \neq 0, \rho)$ energies, respectively. The construction of the phase diagrams is summarized as follows.

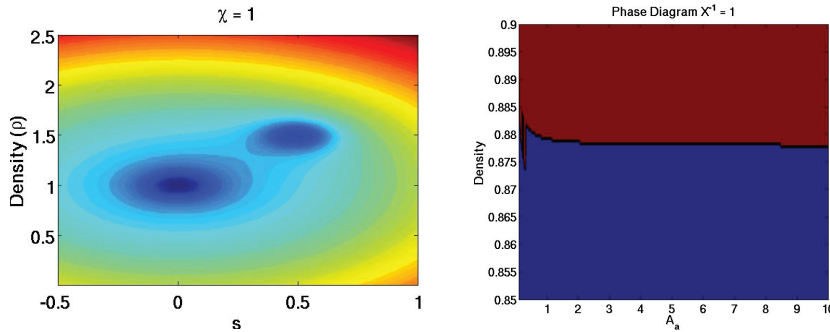


FIG. 5. Contour lines for the bulk potential function (left) and phase space diagram (right) for $\chi = 1$.

1. Construct the bulk energy function $f(s, \rho; \chi)$ for the problem.
2. Define a domain $\mathcal{B} = [\rho_1, \rho_2] \times [A_{a1}, A_{a2}]$ in the *density-aspect-ratio* space.
3. Choose a discrete subset $\mathcal{B}_h \subset \mathcal{B}$ such that

$$\mathcal{B}_h = \{(\rho_1 + ih_1, A_{a1} + jh_2) \mid 0 < h_1 < (\rho_2 - \rho_1), 0 < h_2 < (A_{a2} - A_{a1}) \\ \& i, j \in \mathbb{N}\}.$$

4. Given a point $(\rho_i, A_{ai}) \in \mathcal{B}_h$ compute s by solving the equilibrium equation $\frac{d\mathcal{E}}{ds} = 0$.
5. The point (ρ_i, A_{ai}) is labeled *isotropic* if $\mathcal{E}_{iso} < \mathcal{E}_{nema}$ and *nematic* otherwise.
6. Finally, we plot the nematic and isotropic points in a (ρ, A_a) -diagram. We follow the convention of assigning *red* to nematic points and *blue* to isotropic ones.

We construct f as follows. Let $z := \det F$, and define

$$h(s, z; \chi, s_{i,n}, z_{i,n}, \eta_{i,n}) = \chi W_{iso}(s, z; s_i, z_i, \eta_i) + W_{nema}(s, z; s_n, z_n, \eta_n) \\ + W_{gr}(s, z), \quad (4.14)$$

$$W_{iso}(s, z; s_i, z_i, \eta_i) = \arctan(\eta_i((s - s_i)^2 + (z - z_i)^2)) + (s - s_i)^2 \\ + (z - z_i)^2, \quad (4.15)$$

$$W_{nema}(s, z; s_n, z_n, \eta_n) = \arctan(\eta_n((s - s_n)^2 + (z - z_n)^2)), \quad (4.16)$$

$$W_{gr}(s, z) = -(\log(z) + \log(|s - 1|(s + 0.5))) + z^2. \quad (4.17)$$

The parameters $s_{i,n}, z_{i,n}$ represent the position of the *isotropic* and *nematic* minimum, respectively, and $\eta_{i,n}$ represent the width of the corresponding well. For a fixed set of parameters $\{s_{i,n}, z_{i,n}, \eta_{i,n}\}$, let

$$f(s, \rho; \chi) = h(s, \rho; \chi, s_{i,n}, z_{i,n}, \eta_{i,n}). \quad (4.18)$$

Figures 5 and 6 show phase diagrams for different values of χ and contour plots of $f(s, \rho; \chi)$. A main feature of these diagrams is that the density at which the nematic phase occurs increases with either lowering χ or A_a . (We hold A_a fixed, in the first case, and χ in the latter). Moreover, in these diagrams, the isotropic phase is always present. It would require values $\chi \gg 10^3$ to encounter the nematic phase only. We stipulate that imposing a steeper growth of the energy with respect to ρ , for ρ large, would also yield purely nematic phase diagrams for $\chi = O(10^3)$.

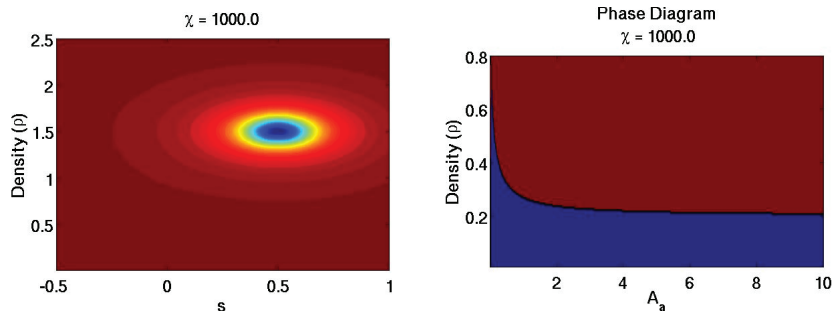


FIG. 6. Contour lines for the bulk potential function (left) and phase space diagram (right) for $\chi = 1000.0$.

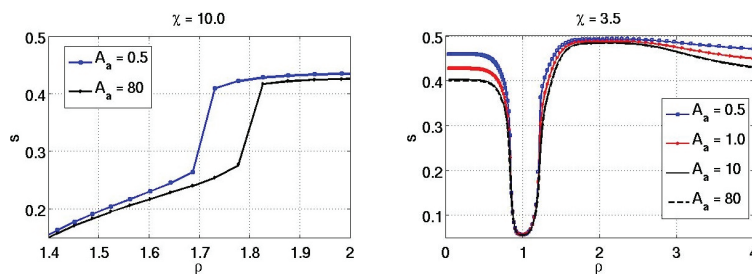


FIG. 7. Order parameter versus density for $\chi = 10$ (left) and $\chi = 3.5$ (right). Nematic well: $s = 0.5$, $\rho = 1.5$. The figure to the right presents a new nematic region at low densities due to the large deformation applied ($\lambda \approx \frac{1}{\rho}$).

4.2.2. Order parameter diagrams and stress-strain plots. Figures 7 and 8 represent plots of the uniaxial order parameter s with respect to the rod density ρ , for $\chi = 0.5, 3.5, 10$, and 80 , and for values of the aspect ratio A_a ranging from 0.01 to 80 . These values represent a range of shapes, from oblate cylinders to very elongated rods. The first graph in Figure 7 presents two density intervals with distinguished behavior, one corresponding to well-aligned rods at high density, with a drop in the uniaxial order parameter as the density decreases to a critical value, and a second interval of further decrease in s as ρ continues decreasing. These graphs are in full agreement with those obtained by Monte Carlo simulations in [6] and [14]. Moreover, the second graph of Figure 7 and those in 8 present a third density interval of increase of the order parameter. This is due to the rod alignment that results from larger extension ratios (i.e., smaller densities), and it is a consequence of the elastic network connections of the rods. Proposition 4.1 shows that this behavior is not analytically predicted when subjecting the material to uniform expansion. It is not reported either in [14]. Another feature that emerges when comparing the two graphs on the right-hand sides of Figures 7 and 8 is that, for larger χ , it is required to reach a lower density to increase the rod alignment. This may indicate the additional difficulty in aligning larger rods, in comparison with smaller ones.

We point out that the first graph in Figure 8 shows the existence of oblate phases of rods with small aspect ratio, in the order of 10^{-2} . This behavior is presented by cytoskeletal networks of red blood cells [3, 9, 36, 37].

We conclude this section discussing the stress-strain Figure 9. For $\chi = 0.5$ and for small and medium values of the rod aspect ratio, the stress-strain curves are monotonic and present a *soft* region followed by a steeper growth. However, we

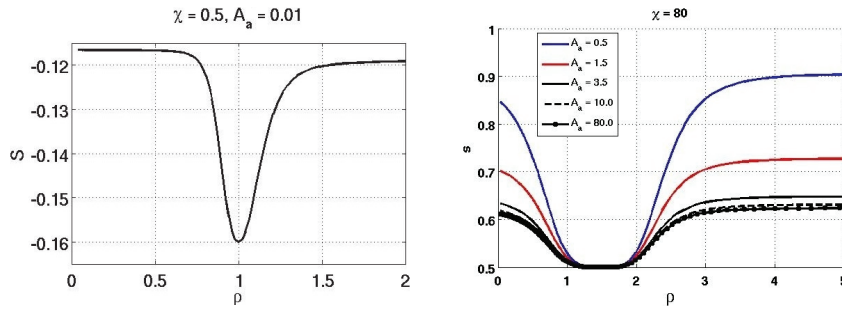


FIG. 8. Order parameter versus density for $\chi = 0.5$ (left) and $\chi = 80$ (right). Nematic well: $s = 0.5$, $\rho = 0.5$.

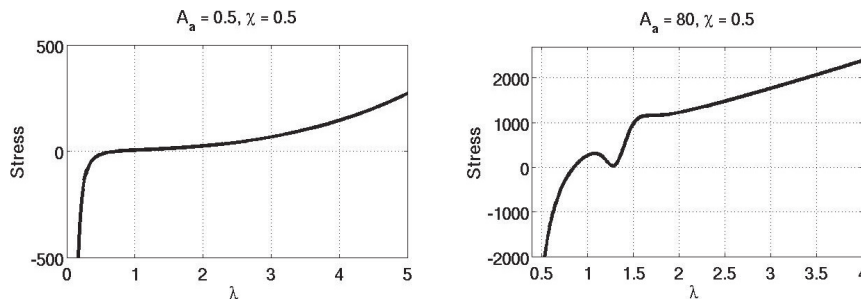


FIG. 9. Plots of the xx -components of the first Piola-Kirchhoff stress tensor.

find that for $A_a = 80$, the stress-strain curves are nonmonotonic. The change of monotonicity occurs precisely where the order parameter experiences a sharp increase or decrease, indicating the change of volume accompanying rod order rearrangement. However, we also found shallower nonmonotonic profiles, including those for systems experiencing the nematic-isotropic phase transition, for aspect ratios smaller than 80. This seems to indicate that realignment of rods with large aspect ratio affects change of volume in a more significant way than for the smaller counterparts.

5. Conclusions. We have presented and analyzed models of anisotropic elasticity based on the theory of liquid crystal elastomers, and applied them to modeling order phase transitions in actin networks. We followed a strategy to show existence of minimizers based on the theory of isotropic nonlinear elasticity. This required assuming that the energy density function is polyconvex with respect to the anisotropic deformation tensor $G = L^{-\frac{1}{2}} \nabla \varphi L_0^{\frac{1}{2}}$. This tensor is at the core of the works on liquid crystal elastomers by Warner and Terentjev.

The assumption that the bulk liquid crystal energy f is a singular potential in Q is an essential ingredient in most of our analysis. Another one is the assumption of a constitutive equation relating the shape of the polymer represented by the tensor L with the order tensor Q of the liquid crystal rigid units. The linear constitutive relation between L and Q guarantees that both tensors become singular at the same asymptotic limit in the order parameter space.

However, the linear relation implicitly involves the constraint of the trace of L being constant and, therefore, it restricts the value of the sum of the principle axis of the ellipsoid associated with L . In future works, we will explore how to avoid this

restriction by assuming nonlinear relations between the two tensors, depending on the availability of experimental data.

In forthcoming work, we aim at constructing bulk free energy functions based on the Onsager rigid rod theory, allowing us to include a variety of molecular symmetries. However, the need to forgo some of the classical approximating expansions that lead to well-known polynomial forms, appears to complicate the task at hand. In thermotropic liquid crystals, the construction of the singular potential (2.26) following the Maier–Saupe theory has been carried out ([5] and also recent work by these authors).

In future work, we will also address the behavior of the system under shearing, consider the case of periodic crosslinking, and include more general forms of the energy capable of describing smectic and lamellar phases, also present in some actin networks.

6. Appendix: Auxiliary results. We present a direct derivation of the results, some of which may have also been independently developed by other researchers.

PROPOSITION 6.1. *Let $L \in \mathbb{S}_+^3$. Then for any matrix $F \in \mathbb{M}^3$*

$$(6.1) \quad \operatorname{tr}(F^T L F) \geq l_{\min}(L) |F|^2,$$

where $l_{\min}(L) > 0$ is the smallest eigenvalue of L .

Proof. Let us consider the spectral decomposition of $L = S^T D S$, where S is an orthogonal matrix and $D = \operatorname{diag}(d_1, d_2, d_3)$ with $0 < d_1 \leq d_2 \leq d_3$. Let us denote $A = S F (S F)^T$ and calculate

$$\begin{aligned} \operatorname{tr}(F^T L F) &= \operatorname{tr}(F^T S^T D S F) = \operatorname{tr}(A D) = \sum_{i=1}^3 d_i A_{ii} \\ &\geq d_1 \sum_i A_{ii} = d_1 \operatorname{tr}(F F^T) = l_{\min}(L) |F|^2, \end{aligned}$$

where we have used the fact that $A_{ii} \geq 0$, for $i = 1, 2, 3$. \square

PROPOSITION 6.2. *Assume $L \in \mathbb{S}_+^3$, then we have*

$$(6.2) \quad \frac{\det(L)}{|L|} \geq \frac{1}{\sqrt{3}} l_{\min}^2(L).$$

Proof. Denoting the eigenvalues of L , $0 < l_1 \leq l_2 \leq l_3$, we have

$$\begin{aligned} |L| &= \sqrt{\operatorname{tr}(L^T L)} \\ &= \sqrt{l_1^2 + l_2^2 + l_3^2}. \end{aligned}$$

Hence

$$\begin{aligned} \frac{\det(L)}{|L|} &= \frac{l_1 l_2 l_3}{\sqrt{l_1^2 + l_2^2 + l_3^2}} \geq \frac{l_1 l_2 l_3}{\sqrt{3} l_3} \\ &= \frac{1}{\sqrt{3}} l_1 l_2 \geq \frac{1}{\sqrt{3}} l_1^2 = \frac{1}{\sqrt{3}} l_{\min}^2(L). \quad \square \end{aligned}$$

LEMMA 6.3. *For given $L, L_0 \in \mathbb{S}_+^3$, let G be as in (2.2). Then the following inequalities hold:*

$$(6.3) \quad |G| \geq C_1 |F|, \quad \text{and}$$

$$(6.4) \quad |\operatorname{adj} G| \geq C_2 |\operatorname{adj} F|,$$

where $C_1 = \sqrt{\frac{l_{\min}(L_0)}{l_{\max}(L)}}$ and $C_2 = \frac{1}{3} C_1^2$.

Proof. We have

$$(6.5) \quad |G|^2 = \operatorname{tr}(L_0 F^T L^{-1} F).$$

Since $L_0 \in \mathbb{S}_+^3$, we let $K_0 = \sqrt{L_0}$. Applying Proposition 6.1, we estimate

$$\begin{aligned} |G|^2 &= \operatorname{tr}(K_0^T F^T L^{-1} F K_0) \\ &\geq l_{\min}(L^{-1}) |F K_0|^2 = l_{\min}(L^{-1}) \operatorname{tr}(F L_0 F^T) \\ &\geq l_{\min}(L^{-1}) l_{\min}(L_0) |F|^2 = \frac{l_{\min}(L_0)}{l_{\max}(L)} |F|^2. \end{aligned}$$

This yields

$$(6.6) \quad |G| \geq \sqrt{\frac{l_{\min}(L_0)}{l_{\max}(L)}} |F|.$$

To prove 6.4, we calculate

$$\begin{aligned} \operatorname{adj}(G) &= \det(G) G^{-1} \\ &= \det(L^{-1/2} F L_0^{1/2}) L_0^{-1/2} F^{-1} L^{1/2} \\ &= \det(L^{-1/2}) \det(L_0^{1/2}) L_0^{-1/2} \operatorname{adj}(F) L^{1/2}. \end{aligned}$$

So

$$(6.7) \quad L_0^{1/2} \operatorname{adj}(G) L^{-1/2} = \det(L^{-1/2}) \det(L_0^{1/2}) \operatorname{adj}(F).$$

By the matrix property $|AB| \leq |A||B|$, we have

$$(6.8) \quad |L_0^{1/2}| \cdot |\operatorname{adj}(G)| \cdot |L^{-1/2}| \geq \det(L^{-1/2}) \det(L_0^{1/2}) |\operatorname{adj}(F)|.$$

Using Proposition 6.2, we have

$$\begin{aligned} |\operatorname{adj}(G)| &\geq \frac{1}{\sqrt{3}} l_{\min}^2(L^{-1/2}) \frac{1}{\sqrt{3}} l_{\min}^2(L_0^{1/2}) |\operatorname{adj}(F)| \\ &= \frac{1}{3} \frac{l_{\min}(L_0)}{l_{\max}(L)} |\operatorname{adj}(F)|. \quad \square \end{aligned}$$

REFERENCES

- [1] V. AGOSTINIANI AND A. DESIMONE, *Ogden-type energies for nematic elastomers*, Internat. J. Nonlinear Mech., 47 (2012), pp. 402–412.
- [2] D. ANDERSON, D. CARLSON, AND E. FRIED, *A continuum-mechanical theory for nematic elastomers*, J. Elasticity, 56 (1999), pp. 33–58.
- [3] P. BAGCHI AND A.Z.K. YAZDANI, *Analysis of membrane tank-tread of nonspherical capsules and red blood cells*, Eur. Phys. J. E Soft Matter Biol. Phys., 35 (2012), pp. 1–12.
- [4] J.M. BALL, *Convexity conditions and existence theorems in nonlinear elasticity*, Arch. Ration. Mech. Anal., 63 (1976), pp. 337–403.
- [5] J.M. BALL AND A. MAJUMDAR, *Nematic liquid crystals: From Maier-Saupe to a continuum theory*, in Mol. Cryst. Liq. Mol., 525 (2010), pp. 1–11.
- [6] M.A. BATES AND D. FRENKEL, *Phase behavior of two-dimensional hard rod fluids*, J. Chem. Phys., 112 (2000), pp. 10034–10041.

- [7] T.J. BYERS AND D. BRANTON, *Visualization of the protein associations in the erythrocyte membrane skeleton*, Proc. Nat. Acad. Sci. USA, 82 (1985), pp. 6153–6157.
- [8] C. LIU AND M.C. CALDERER, *Liquid crystal flow: Dynamic and static configurations*, SIAM J. Appl. Math., 60 (2000), pp. 1925–1949.
- [9] S. CAO, G. WEI, AND J.Z.Y. CHEN, *Transformation of an oblate-shaped vesicle induced by an adhering spherical particle*, Phys. Rev. E (3), 84 (2011), 050901.
- [10] P. CESANA AND A. DESIMONE, *Strain-order coupling in nematic elastomers: Equilibrium configurations*, Math. Models Methods Appl. Sci, 19 (2009), pp. 601–630.
- [11] P. CESANA AND A. DESIMONE, *Quasiconvex envelopes of energies for nematic elastomers in the small strain regime and applications*, J. Mech. Phys. Solids, 59 (2011), pp. 787–803.
- [12] P.G. CIARLET, *Mathematical Elasticity*, Vol. 1, North-Holland, Amsterdam, 1987.
- [13] S. CONTI, A. DESIMONE, AND G. DOLZMANN, *Soft elastic response of stretched sheets of nematic elastomers: A numerical study*, J. Mech. Phys. Solids, 50 (2002), pp. 1431–1451.
- [14] P. DALHAIMER, D.E. DISCHER, AND T.C. LUBENSKY, *Crosslinked actin networks show liquid crystal elastomer behaviour, including soft-mode elasticity*, Nature Phys., 3 (2007), pp. 354–360.
- [15] A. DESIMONE AND G. DOLZMANN, *Material instabilities in nematic elastomers*, Phys. D, 136 (2000), pp. 175–191.
- [16] A. DESIMONE AND G. DOLZMANN, *Macroscopic response of nematic elastomers via relaxation of a class of $SO(3)$ -invariant energies*, Arch. Ration. Mech. Anal., 161 (2002), pp. 181–204.
- [17] A. DESIMONE AND L. TERESI, *Elastic energies for nematic elastomers*, European Phys. J. E Soft Matter Biol. Phys., 29 (2009), pp. 191–204.
- [18] J.L. ERICKSEN, *Liquid crystals with variable degree of orientation*, Arch. Ration. Mech. Anal., 113 (1991), pp. 97–120.
- [19] G. FOREST, Q. WANG, AND R. ZHOU, *A kinetic theory for solutions of nonhomogeneous nematic liquid crystalline polymers with density variations*, J. Fluid Eng., 126 (2004), pp. 180–188.
- [20] E. FRIED AND S. SELLERS, *Free-energy density functions for nematic elastomers*, J. Mech. Phys. Solids, 52 (1999), pp. 1671–1689.
- [21] E. FRIED AND S. SELLERS, *Soft elasticity is not necessary for striping in nematic elastomers*, J. Appl. Phys., 100 (2006), 043521.
- [22] G. FRIESECKE, D.D. JAMES, AND S. MULLER, *A theorem on geometric rigidity and the derivation of nonlinear plate theory from three dimensional elasticity*, Comm. Pure Appl. Math, 55 (2002), pp. 1461–1506.
- [23] F. GAMEZ, S. LAGO, B. GARZON, P. MERKLIN, AND C. VEGA, *Vapour-liquid equilibrium of fluids composed by oblate molecules*, Mol. Phys., 106 (2008), pp. 1331–1339.
- [24] M. GARDEL, J.H. SHIN, L. MAHADEVAN, F.C. MACKINTOSH, P. MATSUDAIRA, AND D.A. WEITZ, *Elastic behavior of cross-linked and bundled actin networks*, Science, 304 (2004), pp. 1301–1305.
- [25] E.F. GRAMSBERGEN, L. LONGA, AND W.H. DE JEU, *Landau theory of nematic isotropic phase transitions*, Phys. Rep., 135 (1986), pp. 197–257.
- [26] J. HAN, W. WANG, AND P. ZHANG, *From microscopic Theory to Macroscopic Theory: A Systematic Study on Static Modeling for Liquid Crystals*, preprint, arXiv:1305.4889, 2013.
- [27] D. HENAO AND C. MORA-CORRAL, *Fracture Surfaces and the Regularity of Inverses for bv Deformations*, Arch. Ration. Mech. Anal., 201 (2011), pp. 575–629.
- [28] M.C. HOLLEY AND J.F. ASHMORE, *A cytoskeletal spring in cochlear outer hair cells*, Nature, 335 (1988), pp. 635–637.
- [29] R. JERRY, A. POPEL, AND W. BROWNELL, *Outer hair cell length changes in an external electric field. i. The role of intracellular electro-osmotically generated pressure gradients*, J. Acoust. Soc. Amer., 98 (1995), pp. 2000–2010.
- [30] J. XU AND P. ZHANG, *From Microscopic Theory to Macroscopic Theory: Symmetries and Order Parameters of Rigid Molecules*, preprint, arXiv:1305.4726, 2013.
- [31] N. KUZUU AND M. DOI, *Constitutive equation for nematic liquid crystals under weak velocity gradient derived from a molecular kinetic equation. I*, J. Phys. Soc. Japan, 52 (1983), pp. 3486–3494.
- [32] N. KUZUU AND M. DOI, *Constitutive equation for nematic liquid crystals under weak velocity gradient derived from a molecular kinetic equation. II*, J. Phys. Soc. Japan, 53 (1984), pp. 1031–1040.
- [33] C. LUO, *Modeling, Analysis and Numerical Simulations of Liquid Crystal Elastomers*, Ph.D. dissertation, University of Minnesota, Minneapolis, MN, 2010.
- [34] A. MAJUMDAR AND A. ZARNESCU, *Landau–De Gennes theory of nematic liquid crystals: The Oseen–Frank limit and beyond*, Arch. Ration. Mech. Anal., 196 (2010), pp. 227–280.
- [35] M.C. CALDERER AND C. LUO, *Numerical study of liquid crystal elastomers by a mixed finite element method*, European J. Appl. Math, 23 (2012), pp. 121–154.

- [36] C. MOHRDIECK, F. DALMAS, E. ARZT, R. THARMANN, M.M.A.E. CLAESSENS, A.R. BAUSCH, A. ROTH, E. SACKMANN, C.H.J. SCHMITZ, J. CURTIS, W. ROOS, K. SCHULZ, S. UHRIG, AND J.P. SPATZ, *Biomimetic models of the actin cytoskeleton*, *Small*, 3 (2007), pp. 1015–1022.
- [37] C. POZRIKIDIS, *The axisymmetric deformation of a red blood cell in uniaxial straining Stokes flow*, *J. Fluid Mech.*, 216 (1990), pp. 231–254.
- [38] A.D. REY, *Liquid crystal models of biological materials and processes*, *Soft Matter*, 6 (2010), pp. 3402–3429.
- [39] G.V. RICHIERI AND S.P. AKESON, *Measurement of biophysical properties of red blood cells by resistive pulse spectroscopy: Volume, shape, surface area, and deformability*, *J. Biochem. Biophys. Methods*, 11 (1985), pp. 117–131.
- [40] B. WAGNER, R. THARMANN, I. HAASE, M. FISCHER, AND A.R. BAUSCH, *Cytoskeletal polymer networks: The molecule structure of cross-linkers determines macroscopic properties. Cochlear outer hair-cells*, *Proc. Natl. Acad. Sci. USA*, 103 (2006), pp. 13974–13978.
- [41] M. WARNER AND E.M. TERENTJEV, *Liquid Crystal Elastomers*, Oxford University Press, Oxford, 2007.
- [42] B. WINCURE AND A.D. REY, *Growth regimes in phase ordering transformations*, *Discrete Contin. Dynam. Systems B*, 8 (2007), pp. 623–648.